Consolidated Competition Ballistics

A Comprehensive Mathematical Manual with Reloading Guide and Julia Implementations

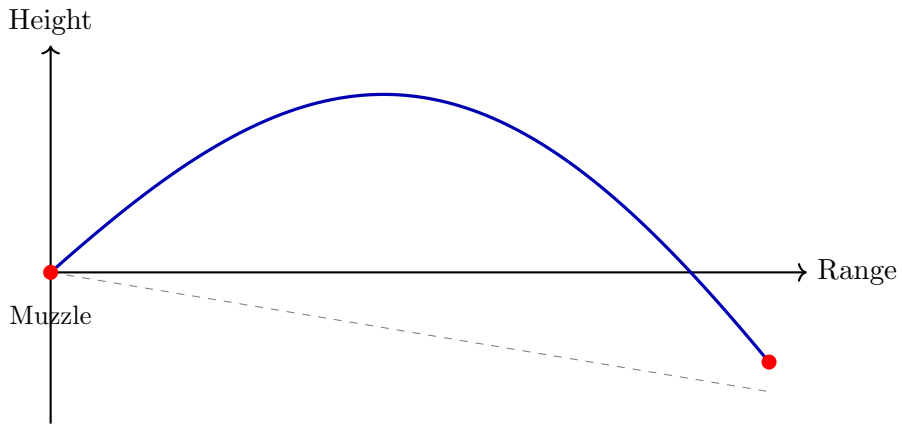

Trajectory with aerodynamic drag and gravity

Merging Core Theory, Advanced Effects, and Practical Shooting Tools
Drag Models (G1–G8), Coriolis & Eötvös Effects, Spin Drift,
Aerodynamic Jump, Wind Deflection, and Handloading Data

Version 3.0 (Consolidated) — May 24, 2026

Contents

Notation and Conventions vii

1 Introduction to Competition Rifle Ballistics 1
- 1.1 Scope and Purpose . . . 1
- 1.2 Overview of Ballistic Phases . . . 1
- 1.3 Historical Context . . . 1

2 Atmospheric Model 3
- 2.1 ICAO Standard Atmosphere . . . 3
  - 2.1.1 Temperature Lapse Rate . . . 3
  - 2.1.2 Pressure–Altitude Relationship . . . 3
- 2.2 Air Density . . . 3
  - 2.2.1 Humidity Correction . . . 4
- 2.3 Speed of Sound . . . 4
- 2.4 Density Altitude . . . 4
- 2.5 Julia Implementation: Atmospheric Model . . . 4

3 Interior Ballistics 7
- 3.1 The Thermodynamic Problem . . . 7
  - 3.1.1 Nobel–Abel Equation of State . . . 7
  - 3.1.2 Energy Balance . . . 7
- 3.2 Simplified Closed-Bomb Model . . . 7
- 3.3 Burn Rate Law . . . 8
  - 3.3.1 Geometric Form Function . . . 8
- 3.4 Le Duc Velocity Model . . . 8
- 3.5 Pressure–Travel Relationship . . . 8
- 3.6 Muzzle Velocity Estimation for Handloaders . . . 9
  - 3.6.1 Temperature Sensitivity of Muzzle Velocity . . . 9

4 Transitional Ballistics 11
- 4.1 Muzzle Gas Dynamics . . . 11
- 4.2 Muzzle Tip-Off and Initial Yaw . . . 11
- 4.3 Base Drag Transition . . . 11
- 4.4 Crown Effects . . . 11

5 Exterior Ballistics: Core Theory 13
- 5.1 Vacuum Trajectory (Baseline) . . . 13
- 5.2 Aerodynamic Drag . . . 13
  - 5.2.1 The Drag Equation . . . 13
  - 5.2.2 Drag Coefficient and Mach Number . . . 14
  - 5.2.3 Analytical Solution for 1D Drag . . . 14
- 5.3 Ballistic Coefficient . . . 15
  - 5.3.1 Standard Conditions for BC . . . 15

5.4 Standard Drag Models (G1 through G8) . . . 15
5.4.1 G7 Drag Function . . . 15
5.5 Doppler Radar Drag Measurement . . . 16
5.5.1 Measurement Principle . . . 16
5.5.2 Extracting $C_{\mathrm{D}}(Ma)$ from Radar Data . . . 16
5.5.3 Advantages over Classical Methods . . . 16
5.5.4 Interpolation of Tabular Drag Data . . . 16
5.6 Equations of Motion: 3-DOF Point-Mass Model . . . 17
5.6.1 Coordinate System . . . 17
5.6.2 Vector Equation of Motion . . . 17
5.6.3 Scalar Component Equations . . . 17
5.6.4 Using the Ballistic Coefficient . . . 18
5.7 Numerical Integration . . . 18
5.7.1 Euler Method . . . 18
5.7.2 Runge–Kutta (RK4) . . . 18

6 Exterior Ballistics: Advanced Effects **19**
6.1 Wind Deflection . . . 19
6.1.1 Wind Components . . . 19
6.1.2 Simple Approximation . . . 19
6.1.3 Lag Rule (Quick Estimation) . . . 19
6.2 Spin Drift . . . 19
6.2.1 Gyroscopic Stability Factor . . . 20
6.3 Coriolis and Eötvös Effects . . . 20
6.3.1 Coriolis Acceleration . . . 20
6.3.2 Horizontal Deflection . . . 20
6.3.3 Vertical Deflection (Eötvös Effect) . . . 20
6.4 Aerodynamic Jump . . . 20
6.5 Magnus Effect . . . 20

7 Complete 3-DOF Ballistic Solver **21**

8 Six-Degree-of-Freedom (6-DOF) Model **23**
8.1 State Vector and Reference Frames . . . 23
8.1.1 Coordinate Systems . . . 23
8.1.2 Euler Angles and Orientation . . . 23
8.1.3 The 12-Component State Vector . . . 23
8.2 Translational Equations of Motion . . . 23
8.2.1 Total Angle of Attack . . . 24
8.2.2 Aerodynamic Force Components . . . 24
8.3 Rotational Equations of Motion . . . 24
8.3.1 Aerodynamic Moments . . . 25
8.3.2 Summary of Moment Components . . . 25
8.4 Kinematic Equations . . . 25
8.5 Quaternion Formulation (Singularity-Free) . . . 25
8.6 Aerodynamic Coefficient Database . . . 26
8.6.1 Typical Values for Match Bullets . . . 26
8.6.2 Deriving C_{D_0} from the Ballistic Coefficient . . . 26
8.7 Moments of Inertia . . . 26
8.8 Spin Rate and Initial Conditions . . . 27
8.9 Stability Revisited from 6-DOF Theory . . . 27
8.9.1 Gyroscopic Stability . . . 27

8.9.2 Dynamic Stability . . . 27
8.10 Comparison: 3-DOF vs. 6-DOF . . . 27
8.11 Julia Implementation: 6-DOF Solver . . . 28

9 Angular Measurement and Sighting Systems 29
9.1 Minute of Angle (MOA) . . . 29
9.2 Milliradian (Mil) . . . 29

10 Reloading Guide for Competition Shooters 31
10.1 Cartridge Selection for Competition . . . 31
10.2 Propellant Selection . . . 31
10.3 Representative Load Data . . . 31
10.4 Complete Worked Example: 6mm BR at 1000 Yards . . . 32
10.4.1 Step 1: Component Data . . . 32
10.4.2 Step 2: Stability Check . . . 33
10.4.3 Step 3: Atmospheric Conditions . . . 33
10.4.4 Step 4: Solver Setup and Trajectory . . . 33
10.4.5 Step 5: Analysis of Results . . . 35
10.4.6 Step 6: Chronograph Validation . . . 35
10.4.7 Step 7: DOPE Card Summary . . . 36
10.5 Interpreting Chronograph Data . . . 36
10.5.1 Velocity SD Impact on Vertical Dispersion . . . 36

11 Ballistic Reference Tables 37
11.1 Bullet Data for Common Competition Bullets . . . 37
11.2 Sample Trajectory Table . . . 37

12 Special Topics 39
12.1 Transonic Stability . . . 39
12.2 Inclined Fire (Rifleman's Rule) . . . 39
12.3 Barrel Harmonics and Optimal Charge Weight . . . 39

13 Error Budget and Sensitivity Analysis 41
13.1 Sensitivity Coefficients . . . 41

14 Ballistic Implications for Reloading 43
14.1 The Reloader's Equation: What You Control . . . 43
14.2 Muzzle Velocity: The Central Reloading Output . . . 43
14.2.1 Charge Weight and Velocity . . . 43
14.2.2 Velocity Consistency and Vertical Dispersion . . . 43
14.2.3 Achieving Low SD: Quantitative Checklist . . . 44
14.3 BC Sensitivity and Bullet Selection . . . 44
14.4 Temperature Effects: Propellant and Atmosphere . . . 44
14.4.1 Combined Temperature Effect . . . 44
14.5 Seating Depth and Internal Ballistic Coupling . . . 44
14.6 Pressure Estimation and Safety Margins . . . 45
14.7 Barrel Life . . . 45
14.8 Load Development Workflow . . . 45

A Detailed Mathematical Derivations 47
A.1 Derivation of the Point-Mass Equations of Motion . . . 47
A.2 Derivation of the Coriolis Terms . . . 47
A.3 Derivation of Spin Drift via Yaw of Repose . . . 47

B Companion Julia Package **49**

C Greenhill's Formula and Twist Rate Selection **51**

Glossary **55**

List of Tables

3.1 Measured muzzle velocity vs. barrel length, .308 Win / Lapua 155 gr Scenar . 9

5.1 BRL Standard Drag Models [McCoy, 1999, Ingalls, 1893] 15
5.2 Selected G7 drag coefficient values [McCoy, 1999] 15

8.1 Typical aerodynamic coefficients for a 6.5 mm 140 gr VLD match bullet . . . 26
8.2 Comparison of 3-DOF and 6-DOF models 27

10.1 Popular competition cartridges and their characteristics 31
10.2 Popular propellants for competition rifle cartridges 31
10.3 6.5 Creedmoor representative loads (24-inch barrel) 32
10.4 .308 Winchester representative loads (24-inch barrel) 32
10.5 6mm Creedmoor representative loads (26-inch barrel) 32
10.6 6mm BR Norma representative loads (26-inch barrel) 32
10.7 Computed trajectory: 6mm BR, 105 gr Berger Hybrid, $v_0 = 2920$ fps, 82 °F, 29.75 in Hg, 55% RH. 8 mph wind at 60°. 100 yd zero. 1:7.5 RH twist, 45.4°N, firing West. 34
10.8 DOPE card: 6mm BR 105 Berger / N140 / 2920 fps. Ottawa, 82 °F, 29.75 inHg. Wind hold is per 1 mph full crosswind. 36
10.9 Typical velocity consistency: factory ammunition vs. optimized handloads . . 36

11.1 Ballistic data for popular competition bullets [Litz, 2011, 2015] 37
11.2 Trajectory: 6.5 CM, 140 gr Berger Hybrid, $\mathrm{BC}_{\mathrm{G7}} = 0.311$, $v_0 = 2700$ fps, 100 yd zero, sea level standard atmosphere 37

12.1 Approximate transonic transition ranges for common competition cartridges at sea-level standard conditions. The transonic zone is defined as $0.9 \leq Ma \leq 1.1$ (≈ 310–$380\ \frac{\mathrm{m}}{\mathrm{s}}$). 39

13.1 Error budget: 6.5 Creedmoor, 140 gr, $\mathrm{BC}_{\mathrm{G7}} = 0.311$, 2700 fps at 1000 yd . . 41

14.1 Velocity sensitivity: vertical shift per 1 fps change, 6.5 CM 140 gr 43
14.2 Estimated velocity SD contributions by reloading variable 44
14.3 Temperature sensitivity by propellant class 44
14.4 SAAMI maximum average pressure for competition cartridges 45
14.5 Approximate barrel life for competition cartridges 45

List of Figures

5.1 Schematic drag coefficient vs. Mach number for G1 and G7 reference projectiles. 14

Notation and Conventions

Throughout this manual, the following conventions are used:

Symbol	Meaning	Typical Units
m	Projectile mass	gr or kg
d	Projectile caliber (diameter)	in or m
v, $\boldsymbol{v}$	Velocity (scalar, vector)	ft/s or $\frac{\text{m}}{\text{s}}$
v_0	Muzzle velocity	ft/s or $\frac{\text{m}}{\text{s}}$
C_D	Drag coefficient (dimensionless)	—
B_C	Ballistic coefficient	$\frac{\text{lbf}}{\text{in}^2}$
SD	Sectional density $= m/d^2$	$\frac{\text{lbf}}{\text{in}^2}$
i or FF	Form factor (dimensionless)	—
ρ	Air density	$\frac{\text{kg}}{\text{m}^3}$
A	Cross-sectional area $= \pi d^2/4$	m^2
g	Gravitational acceleration	$\frac{\text{m}}{\text{s}^2}$
Ma	Mach number $= v/a$	—
a	Local speed of sound	$\frac{\text{m}}{\text{s}}$
T	Temperature	K or °F
P	Barometric pressure	hPa or in Hg
H	Relative humidity	%
θ	Launch (elevation) angle	° or mil
ϕ	Latitude	°
ψ	Azimuth (heading)	°
ω_E	Earth's angular velocity	$7.2921 \times 10^{-5}\ \frac{\text{rad}}{\text{s}}$
S_g	Gyroscopic stability factor	—
τ	Twist rate	in. per turn
r	Range	yd or m
Δy	Vertical drop	in or m
E_k	Kinetic energy	J or ft·lbf

Default values. Parameters shown in [default: blue brackets] indicate default values used when the specific value is unknown. These are based on ICAO standard atmosphere and common competition shooting conditions.

Unit systems. All derivations use SI units internally. Conversion factors to Imperial units (grains, feet per second, inches, etc.) are provided throughout.

Chapter 1

Introduction to Competition Rifle Ballistics

1.1 Scope and Purpose

This manual provides a rigorous mathematical treatment of the ballistic phenomena relevant to precision rifle competition, including but not limited to: F-Class, Palma, Benchrest, PRS (Precision Rifle Series), NRL (National Rifle League), High-Power, and long-range target shooting. The goal is to equip the competitive shooter with both the theoretical foundations and the practical computational tools needed to predict bullet trajectories to the highest possible accuracy.

Competition shooting demands sub-MOA accuracy at distances often exceeding 1000 yd. At these ranges, small errors in modeling atmospheric drag, spin drift, Coriolis deflection, or wind become dominant factors in the miss distance. This manual addresses each of these systematically.

1.2 Overview of Ballistic Phases

The flight of a bullet from ignition to impact is conventionally divided into four phases [McCoy, 1999]:

1. **Interior Ballistics** — The physics of the bullet inside the barrel, from primer ignition through propellant combustion to muzzle exit. Key outputs: muzzle velocity, chamber pressure, barrel time.
2. **Transitional (Intermediate) Ballistics** — The brief phase as the bullet exits the muzzle and the propellant gases dissipate. Muzzle blast interaction, base drag changes, and initial yaw (tip-off) are determined here.
3. **Exterior Ballistics** — The free-flight trajectory from muzzle to target. This is the dominant focus of competition ballistics: aerodynamic drag, gravity drop, wind deflection, spin drift, Coriolis and Eötvös effects, Magnus force, and aerodynamic jump.
4. **Terminal Ballistics** — Bullet behavior at impact. While less critical for paper-target competition, terminal effects matter for steel-target energy requirements and for hunting-oriented competitions.

1.3 Historical Context

The mathematical study of projectile motion dates to Galileo and Newton, but modern exterior ballistics began with the work of Bashforth (1870), who conducted some of the earliest systematic drag measurements [Bashforth, 1870]. The Siacci method (1880s) introduced the concept of the ballistic coefficient and drag functions that remain in use today [Siacci,

1888]. In the 20th century, the US Army Ballistic Research Laboratory (BRL) at Aberdeen Proving Ground produced the definitive drag function tables—G1 through G8—that form the backbone of modern ballistic computation [McCoy, 1999, Ingalls, 1893].

Modern computational ballistics, exemplified by solvers such as those described by Litz [2011] and implemented in software like Bryan Litz's Applied Ballistics suite, use 3-DOF and 6-DOF point-mass models with empirically measured drag data and atmospheric corrections.

Chapter 2

Atmospheric Model

The atmosphere is the medium through which the bullet travels. Accurate modeling of air density, speed of sound, and viscosity is prerequisite to all exterior ballistic calculations.

2.1 ICAO Standard Atmosphere

The International Civil Aviation Organization (ICAO) standard atmosphere defines baseline conditions at sea level [ICAO, 1993]:

$$T_0 = 288.15\,\mathrm{K} \quad (59\,^\circ\mathrm{F}) \tag{2.1}$$
$$P_0 = 101\,325\,\mathrm{Pa} \quad (29.92\ \mathrm{in\ Hg}) \tag{2.2}$$
$$\rho_0 = 1.2250\,\frac{\mathrm{kg}}{\mathrm{m}^3} \tag{2.3}$$
$$a_0 = 340.294\,\frac{\mathrm{m}}{\mathrm{s}} \quad (1116.45\,\mathrm{ft/s}) \tag{2.4}$$
$$H_0 = 0\% \quad (\mathrm{dry\ air}) \tag{2.5}$$

Default values: $T_0 = 288.15$ K, $P_0 = 101325$ Pa, $\rho_0 = 1.225$ kg/m^3, $H_0 = 0\%$.

2.1.1 Temperature Lapse Rate

Below 11 000 m (troposphere), the standard lapse rate is:

$$T(h) = T_0 - L \cdot h, \qquad L = 0.0065\,\frac{\mathrm{K}}{\mathrm{m}} \tag{2.6}$$

where h is the altitude above sea level in meters.

2.1.2 Pressure–Altitude Relationship

Using the barometric formula for the troposphere:

$$P(h) = P_0 \left(\frac{T(h)}{T_0} \right)^{g_0/(L\,R_{\mathrm{air}})} = P_0 \left(1 - \frac{L\,h}{T_0} \right)^{5.2559} \tag{2.7}$$

where $g_0 = 9.806\,65\ \frac{\mathrm{m}}{\mathrm{s}^2}$ and $R_{\mathrm{air}} = 287.058\ \frac{\mathrm{J}}{\mathrm{kg \cdot K}}$.

2.2 Air Density

The ideal gas law gives the dry-air density:

$$\rho_{\mathrm{dry}} = \frac{P}{R_{\mathrm{air}}\,T} \tag{2.8}$$

2.2.1 Humidity Correction

Humid air is *less dense* than dry air because water vapor ($M_w = 18.015\,\frac{\text{g}}{\text{mol}}$) is lighter than diatomic nitrogen ($M_{N_2} = 28.014\,\frac{\text{g}}{\text{mol}}$) and oxygen ($M_{O_2} = 31.998\,\frac{\text{g}}{\text{mol}}$).

The saturation vapor pressure (August–Roche–Magnus formula):

$$e_s(T) = 6.1078 \times 10^{\frac{7.5\,(T-273.15)}{T-35.85}} \quad \text{[hPa]} \tag{2.9}$$

The partial pressure of water vapor:

$$e = \frac{H}{100}\, e_s(T) \tag{2.10}$$

Corrected density accounting for humidity (virtual temperature method):

$$\rho = \frac{P - 0.3783\, e}{R_{\text{air}}\, T} \tag{2.11}$$

The factor 0.3783 arises from $(1 - M_w/M_{\text{air}}) = 1 - 18.015/28.964 \approx 0.3780$.

2.3 Speed of Sound

The speed of sound in air depends primarily on temperature:

$$a = \sqrt{\gamma\, R_{\text{air}}\, T} = 20.0468\,\sqrt{T} \tag{2.12}$$

where $\gamma = 1.4$ is the ratio of specific heats for air.

At the ICAO standard temperature: $a_0 = 20.0468\sqrt{288.15} = 340.29\,\frac{\text{m}}{\text{s}}$.

2.4 Density Altitude

Shooters often use density altitude (DA) as a single parameter that encapsulates the combined effects of temperature, pressure, and humidity on air density. DA is the altitude in the standard atmosphere that has the same density as the actual conditions:

$$\text{DA} = \frac{T_0}{L}\left[1 - \left(\frac{\rho}{\rho_0}\right)^{1/(n-1)}\right] \tag{2.13}$$

where $n = g_0/(L\, R_{\text{air}}) + 1 = 6.2559$.

A practical approximation widely used in the field [Litz, 2011]:

$$\text{DA} \approx 145442.16\left(1 - \left(\frac{\rho}{\rho_0}\right)^{0.234969}\right) \quad \text{[feet]} \tag{2.14}$$

2.5 Julia Implementation: Atmospheric Model

```
# See CompetitionBallistics.jl, module Atmosphere
# Key functions:
#   std_temperature(h)            -> T [K]
#   std_pressure(h)               -> P [Pa]
#   air_density(; P, T, H)        -> rho [kg/m^3]
```

```
6 #    speed_of_sound(T)              -> a [m/s]
7 #    density_altitude(rho)          -> DA [m]
8 #    saturation_vapor_pressure(T) -> e_s [Pa]
```

Listing 2.1: Atmospheric model in Julia

Chapter 3

Interior Ballistics

Interior ballistics governs the conversion of chemical energy stored in propellant into kinetic energy of the projectile. For the competition shooter, the key outputs are muzzle velocity and its consistency (extreme spread and standard deviation).

3.1 The Thermodynamic Problem

3.1.1 Nobel–Abel Equation of State

Propellant gases at high pressure deviate significantly from ideal-gas behavior. The Nobel–Abel equation accounts for the finite co-volume of gas molecules [McCoy, 1999, Carlucci and Jacobson, 2007]:

$$P\,(V - \eta) = n\,R_u\,T_g \tag{3.1}$$

where P is the chamber pressure, V is the gas volume, $\eta = n\,b$ is the total co-volume, n is the number of moles of gas, $R_u = 8.3145\ \frac{\text{J}}{\text{mol}\cdot\text{K}}$ is the universal gas constant, and T_g is the gas temperature.

3.1.2 Energy Balance

The first law of thermodynamics applied to the propellant–projectile system:

$$Q_{\text{prop}} = E_k + E_{\text{heat}} + E_{\text{friction}} + E_{\text{gas KE}} + E_{\text{residual}} \tag{3.2}$$

The total chemical energy released by the propellant charge:

$$Q_{\text{prop}} = C \cdot f \cdot z \tag{3.3}$$

where C is the charge mass, f is the impetus (force constant, energy per unit mass), and z is the fraction of charge burned ($0 \le z \le 1$).

3.2 Simplified Closed-Bomb Model

In a closed bomb (no projectile motion), the pressure is:

$$P = \frac{C\,f\,z}{V_{\text{ch}} - C\,(1 - z)/\rho_p - C\,z\,\eta_{\text{sp}}} \tag{3.4}$$

where V_{ch} is the chamber volume, ρ_p is the solid propellant density, and η_{sp} is the specific co-volume.

3.3 Burn Rate Law

The rate of gas generation follows a geometric burn rate law. For a single-perforated cylindrical grain:

$$\frac{\mathrm{d}z}{\mathrm{d}t} = \frac{S(z)}{V_g(z)}\,\beta\,P^n \tag{3.5}$$

For small arms propellants, the empirical Vielle law is commonly used:

$$r_b = \beta\,P^n \tag{3.6}$$

where r_b is the linear regression rate ($\frac{\mathrm{m}}{\mathrm{s}}$), and typical values are $n \approx 0.6$–0.9.

3.3.1 Geometric Form Function

For common grain geometries, the fraction burned z relates to the linear fraction burned $\xi = e/e_0$ through a form function:

$$z(\xi) = \xi\,(1 + \theta\,\xi) \tag{3.7}$$

where θ is the form factor: $\theta = 0$ for a slab, $\theta > 0$ for progressive, and $\theta < 0$ for degressive grains.

3.4 Le Duc Velocity Model

A classical approximation for muzzle velocity useful for handloading estimates [McCoy, 1999]:

$$v(x) = \frac{a\,x}{b + x} \tag{3.8}$$

where x is the projectile travel distance from the cartridge case mouth, and a and b are empirically determined constants. As $x \to \infty$, $v \to a$, so a represents the theoretical maximum velocity.

3.5 Pressure–Travel Relationship

The pressure as a function of bullet travel x in the barrel:

$$P(x) = \frac{m_e}{A_{\mathrm{bore}}}\,\frac{\mathrm{d}v}{\mathrm{d}t} = \frac{m_e\,v}{A_{\mathrm{bore}}}\,\frac{\mathrm{d}v}{\mathrm{d}x} \tag{3.9}$$

where $m_e = m + C/3$ is the effective mass and $A_{\mathrm{bore}} = \pi d^2/4$ is the bore cross-sectional area.

Using the Le Duc model, the pressure becomes:

$$P(x) = \frac{m_e\,a^2\,b\,x}{A_{\mathrm{bore}}\,(b + x)^3} \tag{3.10}$$

The peak pressure occurs at $x_{\max} = b/2$:

$$P_{\max} = \frac{4\,m_e\,a^2}{27\,A_{\mathrm{bore}}\,b} \tag{3.11}$$

3.6 Muzzle Velocity Estimation for Handloaders

A practical empirical formula due to Powley and refined by Litz [2011]:

$$v_0 \approx v_{\text{ref}} \left(\frac{L_{\text{barrel}}}{L_{\text{ref}}} \right)^{0.25 \text{ to } 0.30} \tag{3.12}$$

A rough rule of thumb: each inch of barrel length change alters muzzle velocity by approximately 20 ft/s to 35 ft/s for typical rifle cartridges [Litz, 2011].

As a practical validation of Eq. (3.12), consider measured data for the .308 Winchester with Lapua 155 gr Scenar ammunition:

Table 3.1: Measured muzzle velocity vs. barrel length, .308 Win / Lapua 155 gr Scenar

Barrel length (in)	v_0 **(m/s)**	v_0 **(fps)**
20	820	2690
24	845	2772
26	860	2822

This yields approximately 12 $\frac{\text{m}}{\text{s}}$ ($\approx$40 ft/s) per additional inch beyond 20 inches, which is consistent with the power-law exponent of 0.27 used in the companion Julia library. Note that the gain per inch diminishes with longer barrels, as the propellant gas expansion cools and pressure drops.

3.6.1 Temperature Sensitivity of Muzzle Velocity

Propellant burn rate is temperature-dependent. The temperature coefficient:

$$\frac{\Delta v_0}{v_0} = \sigma_T \, \Delta T \tag{3.13}$$

where σ_T is the temperature sensitivity coefficient, typically 0.5 to 2.0 fps/°F depending on propellant. Modern temperature-stable propellants like Hodgdon Extreme series have $\sigma_T \approx 0.5$ fps/°F [Litz, 2011].

[default: $\sigma_T = 1.0$ fps/°F]

Chapter 4

Transitional Ballistics

Transitional (or intermediate) ballistics covers the brief period after the bullet exits the muzzle and before it settles into free flight. This phase lasts only a few calibers of travel but establishes critical initial conditions for the exterior trajectory.

4.1 Muzzle Gas Dynamics

When the bullet exits the barrel, the high-pressure propellant gases (10–70 MPa) expand rapidly into the atmosphere. The gas jet initially travels faster than the bullet and forms a complex shock-wave structure [Carlucci and Jacobson, 2007]:

1. **Muzzle blast wave**: A spherical shock radiating outward.
2. **Precursor blast**: From air compressed ahead of the bullet in the barrel.
3. **Bottle shock**: The characteristic diamond-pattern Mach disk structure formed by the underexpanded supersonic gas jet.

4.2 Muzzle Tip-Off and Initial Yaw

As the bullet exits the muzzle, asymmetric gas forces can impart a small angular velocity (tip-off rate). The resulting initial yaw angle α_0 is typically small (0.5–3 °F) for well-made ammunition but is a significant factor in group size.

4.3 Base Drag Transition

Inside the barrel, the bullet base is subject to gas pressure. Upon exit, this pressure rapidly drops to ambient, and base drag increases significantly. The base drag coefficient transitions from a suppressed value to its free-flight value over a distance of approximately 5–20 calibers from the muzzle [McCoy, 1999].

4.4 Crown Effects

The muzzle crown—the precise geometry at the barrel's end—is critical to accuracy because it determines how symmetrically the gases release around the bullet base.

Chapter 5

Exterior Ballistics: Core Theory

This chapter develops the mathematical framework for predicting the bullet's trajectory in free flight.

5.1 Vacuum Trajectory (Baseline)

In the absence of air resistance, the trajectory is a simple parabola. This model is useful as a theoretical baseline but is *insufficient for real-world ballistics* because bullets travel at supersonic speeds where aerodynamic drag dominates the behavior. Precision rifle shooting relies on understanding the physics governing projectile motion beyond the idealized vacuum case, accounting for gravity, drag, wind, and spin.

The equations of motion in vacuum are:

$$x(t) = v_0 \cos\theta \cdot t \tag{5.1}$$

$$y(t) = v_0 \sin\theta \cdot t - \frac{1}{2} g\, t^2 \tag{5.2}$$

Eliminating t from Eq. (5.1) and substituting into Eq. (5.2) yields the trajectory equation in terms of horizontal distance x:

$$\boxed{y(x) = x \tan\theta - \frac{g x^2}{2 v_0^2 \cos^2\theta}} \tag{5.3}$$

The range in vacuum:

$$R_{\text{vac}} = \frac{v_0^2 \sin 2\theta}{g} \tag{5.4}$$

5.2 Aerodynamic Drag

5.2.1 The Drag Equation

The aerodynamic drag force opposes the bullet's motion through the air:

$$\boxed{F_D = \frac{1}{2}\, \rho\, v^2\, C_{\text{D}}(Ma)\, A} \tag{5.5}$$

The drag deceleration:

$$a_D = \frac{F_D}{m} = \frac{\rho\, v^2\, C_{\text{D}}\, A}{2\, m} \tag{5.6}$$

5.2.2 Drag Coefficient and Mach Number

The drag coefficient C_{D} is fundamentally a function of Mach number $Ma = v/a$, Reynolds number Re, and projectile geometry. For small-arms bullets, Re effects are secondary, and C_{D} is treated as a function of Ma alone [McCoy, 1999].

The C_{D}–Ma curve has characteristic regimes: subsonic ($Ma < 0.8$) with low, slowly varying C_{D}; transonic ($0.8 < Ma < 1.2$) with a sharp rise; and supersonic ($Ma > 1.2$) with gradually decreasing C_{D}.

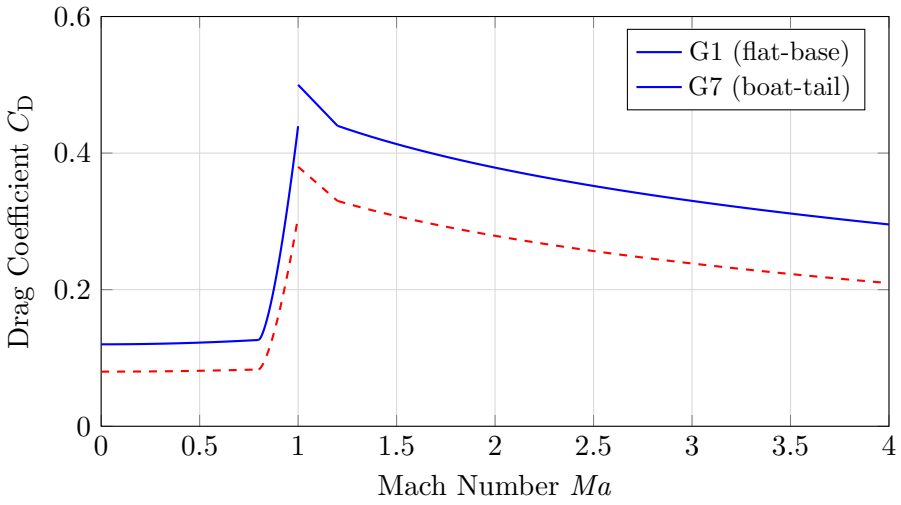

Figure 5.1: Schematic drag coefficient vs. Mach number for G1 and G7 reference projectiles.

5.2.3 Analytical Solution for 1D Drag

While modern ballistics requires numerical integration (see Section 5.7), a simplified 1D model where C_{D} is assumed constant provides useful insights into the scaling of range and velocity with respect to the ballistic coefficient.

Consider purely horizontal motion with drag as the only force:

$$\frac{\mathrm{d}v}{\mathrm{d}t} = -k\,v^2, \quad \text{where } k = \frac{\rho\, C_{\mathrm{D}}\, A}{2\,m} \tag{5.7}$$

Separating variables and integrating:

$$\int_{v_0}^{v} \frac{\mathrm{d}v'}{(v')^2} = -k \int_0^t \mathrm{d}t' \implies -\left[\frac{1}{v'}\right]_{v_0}^{v} = -k\,t \tag{5.8}$$

The velocity as a function of time is:

$$\boxed{v(t) = \frac{v_0}{1 + k\,v_0\,t}} \tag{5.9}$$

Integrating once more to find the distance $x(t)$:

$$x(t) = \int_0^t \frac{v_0}{1 + k\,v_0\,t'}\mathrm{d}t' = \frac{1}{k}\ln(1 + k\,v_0\,t) \tag{5.10}$$

Solving for t in terms of x:

$$t = \frac{e^{kx} - 1}{k\,v_0} \tag{5.11}$$

Substituting this into Eq. (5.9) yields the velocity as a function of distance:

$$\boxed{v(x) = v_0 e^{-kx}} \tag{5.12}$$

This exponential decay demonstrates how the "Physics BC" (contained within k) determines the velocity retention of the projectile.

5.3 Ballistic Coefficient

The ballistic coefficient B_{C} is defined as:

$$\boxed{B_{\mathrm{C}} = \frac{\mathrm{SD}}{i} = \frac{m}{i\,d^2}} \tag{5.13}$$

where $\mathrm{SD} = m/d^2$ is the sectional density and i is the form factor:

$$i(Ma) = \frac{C_{\mathrm{D}}^{\mathrm{bullet}}(Ma)}{C_{\mathrm{D}}^{\mathrm{std}}(Ma)} \tag{5.14}$$

B_{C} is only meaningful when referenced to a specific drag model (G1, G7, etc.).

5.3.1 Standard Conditions for BC

By convention, B_{C} values are quoted at standard atmosphere conditions. To use B_{C} at non-standard conditions:

$$B_{C\,\mathrm{actual}} = B_{C\,\mathrm{std}} \cdot \frac{\rho_0}{\rho_{\mathrm{actual}}} \tag{5.15}$$

5.4 Standard Drag Models (G1 through G8)

Table 5.1: BRL Standard Drag Models [McCoy, 1999, Ingalls, 1893]

Model	**Reference Projectile Shape**	**Primary Use**
G1	Flat-base with 2-caliber ogive nose	Traditional default; hunting bullets
G7	Long, secant-ogive, boat-tail	**Best for modern VLD match bullets**
G8	Similar to G7 with flat base	Flat-base match bullets
GL	Blunt-nose lead bullet	Cast lead bullets

For competition rifle shooting, G7 is strongly preferred over G1 for modern VLD boat-tail bullets because the G7 reference shape more closely matches these bullets, resulting in a form factor i closer to 1.0 and a more constant B_{C} across the velocity range [Litz, 2011].

5.4.1 G7 Drag Function

Table 5.2: Selected G7 drag coefficient values [McCoy, 1999]

Ma	$C_{\mathrm{D}}^{\mathrm{G7}}$	Ma	$C_{\mathrm{D}}^{\mathrm{G7}}$	Ma	$C_{\mathrm{D}}^{\mathrm{G7}}$
0.00	0.1198	1.00	0.4002	2.00	0.2487
0.50	0.1198	1.05	0.3810	2.50	0.2169
0.80	0.1280	1.10	0.3621	3.00	0.1966
0.90	0.1687	1.20	0.3278	3.50	0.1800
0.95	0.2300	1.50	0.2860	4.00	0.1668

5.5 Doppler Radar Drag Measurement

The drag coefficient tables (G1, G7, etc.) originate from experimental measurements. The modern gold standard is *Doppler radar tracking*, which has largely superseded earlier spark-range and yaw-card methods [McCoy, 1999, Braun, 1958].

5.5.1 Measurement Principle

A continuous-wave (CW) Doppler radar illuminates the bullet in flight and measures the frequency shift of the reflected signal:

$$f_D = \frac{2\,v\,\cos\theta_r}{\lambda} \tag{5.16}$$

where f_D is the Doppler shift frequency, v is the bullet velocity, θ_r is the angle between the velocity vector and the radar beam, and λ is the radar wavelength. The velocity is sampled at rates of 1–10 kHz, yielding a near-continuous $v(t)$ record over the entire flight.

5.5.2 Extracting $C_{\mathrm{D}}(Ma)$ from Radar Data

From the measured velocity–time history, the drag coefficient is extracted by inverting the equation of motion. For a near-horizontal trajectory:

$$C_{\mathrm{D}}(Ma) = -\frac{2\,m}{\rho\,A\,v^2}\,\frac{\mathrm{d}v}{\mathrm{d}t} \tag{5.17}$$

The derivative $\mathrm{d}v/\mathrm{d}t$ is computed numerically from the sampled $v(t)$ data. Since numerical differentiation amplifies noise, the raw data is first smoothed using a Savitzky–Golay filter or a cubic smoothing spline before differentiation.

The Mach number at each time step is:

$$Ma(t) = \frac{v(t)}{a\big(T(h(t))\big)} \tag{5.18}$$

where a is the local speed of sound, corrected for the altitude $h(t)$ along the trajectory.

5.5.3 Advantages over Classical Methods

Doppler radar provides the complete $C_{\mathrm{D}}(Ma)$ curve from a *single firing*, whereas spark-range methods require many shots at different velocities. This is the method used by:

- The BRL/ARL at Aberdeen Proving Ground to produce the definitive G1–G8 tables.
- Bryan Litz (Applied Ballistics) to measure custom drag curves for individual bullet models, published as "CDM" (Custom Drag Model) data [Litz, 2015].
- Military proving grounds worldwide for projectile development.

The custom drag model approach bypasses the form-factor approximation entirely: instead of $C_{\mathrm{D}} = i \cdot C_{\mathrm{D}}^{\mathrm{std}}$, the actual measured $C_{\mathrm{D}}(Ma)$ curve for the specific bullet is used directly. This eliminates the error from form-factor variation with Mach number and is the most accurate approach available.

5.5.4 Interpolation of Tabular Drag Data

Whether using the standard G1/G7 tables or a custom Doppler-derived curve, the drag coefficient must be evaluated at arbitrary Mach numbers during trajectory integration. Two interpolation methods are common:

Linear interpolation (used in many legacy solvers): Given tabular data $\{(Ma_i, C_{D,i})\}$, find the bracketing interval $[Ma_k, Ma_{k+1}]$ and compute:

$$C_{\mathrm{D}}(Ma) = C_{D,k} + \frac{C_{D,k+1} - C_{D,k}}{Ma_{k+1} - Ma_k}\,(Ma - Ma_k) \tag{5.19}$$

Linear interpolation introduces slope discontinuities at each table point. In the transonic region where C_{D} changes rapidly, these discontinuities can produce small but systematic trajectory errors.

Cubic spline interpolation (recommended): A natural cubic spline $S(Ma)$ is fitted through all n data points, producing a C^2-continuous curve (continuous through the second derivative). The spline on each interval $[Ma_k, Ma_{k+1}]$ is:

$$S(Ma) = a_k + b_k\,(Ma - Ma_k) + c_k\,(Ma - Ma_k)^2 + d_k\,(Ma - Ma_k)^3 \tag{5.20}$$

where the coefficients $\{a_k, b_k, c_k, d_k\}$ are determined by enforcing continuity of S, S', and S'' at interior knots, plus natural boundary conditions ($S'' = 0$ at endpoints). This requires solving a tridiagonal linear system of size n, which is $O(n)$ and needs to be done only once during initialization.

Cubic spline interpolation is particularly important in the transonic region ($0.9 < Ma < 1.2$) where the C_{D} curve has its steepest gradient. The smooth derivative ensures that the drag force varies smoothly as the bullet decelerates through the sound barrier, eliminating artificial trajectory perturbations.

The companion Julia implementation (Appendix B) provides both linear and cubic spline interpolation via the `DragModels` module.

5.6 Equations of Motion: 3-DOF Point-Mass Model

5.6.1 Coordinate System

We use a ground-fixed, flat-Earth coordinate system: x (downrange), y (vertical, upward positive), z (cross-range, positive right).

5.6.2 Vector Equation of Motion

$$\boxed{m\,\frac{\mathrm{d}\boldsymbol{v}}{\mathrm{d}t} = -\frac{1}{2}\,\rho\,\|\boldsymbol{v}_{\mathrm{rel}}\|\,\boldsymbol{v}_{\mathrm{rel}}\,C_{\mathrm{D}}(Ma)\,A + m\,\boldsymbol{g}} \tag{5.21}$$

where $\boldsymbol{v}_{\mathrm{rel}} = \boldsymbol{v} - \boldsymbol{v}_{\mathrm{wind}}$ and $\boldsymbol{g} = (0, -g, 0)^T$.

5.6.3 Scalar Component Equations

$$\frac{\mathrm{d}v_x}{\mathrm{d}t} = -\frac{\rho\,C_{\mathrm{D}}\,A}{2\,m}\,v_{\mathrm{rel}}\,(v_x - w_x) \tag{5.22}$$

$$\frac{\mathrm{d}v_y}{\mathrm{d}t} = -\frac{\rho\,C_{\mathrm{D}}\,A}{2\,m}\,v_{\mathrm{rel}}\,(v_y - w_y) - g \tag{5.23}$$

$$\frac{\mathrm{d}v_z}{\mathrm{d}t} = -\frac{\rho\,C_{\mathrm{D}}\,A}{2\,m}\,v_{\mathrm{rel}}\,(v_z - w_z) \tag{5.24}$$

where $v_{\mathrm{rel}} = \sqrt{(v_x - w_x)^2 + (v_y - w_y)^2 + (v_z - w_z)^2}$.

5.6.4 Using the Ballistic Coefficient

Substituting $C_\mathrm{D} = i \cdot C_\mathrm{D}^\mathrm{std}$ and $B_\mathrm{C} = m/(i\,d^2)$:

$$\frac{\rho\, C_\mathrm{D}\, A}{2\,m} = \frac{\rho\, C_\mathrm{D}^\mathrm{std}\, \pi}{8\, B_\mathrm{C}} \tag{5.25}$$

5.7 Numerical Integration

Since the system of equations (Eqs. 5.22–5.24) has no closed-form solution due to the non-linear dependence of C_D on velocity, it must be solved numerically.

5.7.1 Euler Method

The simplest numerical approach is the first-order Euler method, which updates the state vector using the derivative at the beginning of each time step Δt:

$$v_x^{n+1} = v_x^n + \Delta t \left(-\frac{\rho\, C_\mathrm{D}\, A}{2\,m}\, v^n\, (v_x^n - w_x) \right) \tag{5.26}$$

$$v_y^{n+1} = v_y^n + \Delta t \left(-\frac{\rho\, C_\mathrm{D}\, A}{2\,m}\, v^n\, (v_y^n - w_y) - g \right) \tag{5.27}$$

$$x^{n+1} = x^n + v_x^n\, \Delta t \tag{5.28}$$

$$y^{n+1} = y^n + v_y^n\, \Delta t \tag{5.29}$$

where $v^n = \sqrt{(v_x^n - w_x)^2 + (v_y^n - w_y)^2 + (v_z^n - w_z)^2}$. While intuitive and easy to implement, the Euler method requires very small time steps to maintain stability and accuracy.

5.7.2 Runge–Kutta (RK4)

Modern ballistic solvers use higher-order methods, typically the 4th-order Runge–Kutta (RK4) method, which provides a much better balance of speed and precision by sampling the derivative at multiple points within the time step [Press et al., 2007]:

$$\boldsymbol{k}_1 = h\, \boldsymbol{f}(t_n, \boldsymbol{y}_n) \tag{5.30}$$

$$\boldsymbol{k}_2 = h\, \boldsymbol{f}(t_n + h/2, \boldsymbol{y}_n + \boldsymbol{k}_1/2) \tag{5.31}$$

$$\boldsymbol{k}_3 = h\, \boldsymbol{f}(t_n + h/2, \boldsymbol{y}_n + \boldsymbol{k}_2/2) \tag{5.32}$$

$$\boldsymbol{k}_4 = h\, \boldsymbol{f}(t_n + h, \boldsymbol{y}_n + \boldsymbol{k}_3) \tag{5.33}$$

$$\boldsymbol{y}_{n+1} = \boldsymbol{y}_n + \tfrac{1}{6}(\boldsymbol{k}_1 + 2\boldsymbol{k}_2 + 2\boldsymbol{k}_3 + \boldsymbol{k}_4) \tag{5.34}$$

A typical time step of $h = 0.0005$ to $0.001\,\mathrm{s}$ is sufficient.

Chapter 6

Exterior Ballistics: Advanced Effects

6.1 Wind Deflection

Wind is the single largest variable in long-range competition shooting.

6.1.1 Wind Components

Given wind speed W at angle α_w relative to the line of fire:

$$w_x = -W \cos \alpha_w \quad \text{(headwind/tailwind)} \tag{6.1}$$

$$w_z = W \sin \alpha_w \quad \text{(crosswind)} \tag{6.2}$$

6.1.2 Simple Approximation

A crude but sometimes useful first-order approximation for lateral drift (crosswind drift) is:

$$\Delta z_{\text{wind}} \approx \frac{W \sin \alpha_w}{v_{\text{avg}}} \cdot R \tag{6.3}$$

where v_{avg} is the average velocity over the range R. This model assumes the bullet instantly acquires the transverse velocity of the wind, which is physically unrealistic for high-velocity projectiles.

6.1.3 Lag Rule (Quick Estimation)

The Didion approximation, also known as the Lag Rule [McCoy, 1999, Litz, 2011]:

$$\Delta z_{\text{wind}} \approx W \sin \alpha_w \cdot \left(t_{\text{actual}} - \frac{R}{v_0 \cos \theta} \right) \tag{6.4}$$

This is remarkably accurate (within 5%) and provides an intuitive physical picture: the wind deflection equals the crosswind speed multiplied by the lag time that drag has cost the bullet.

6.2 Spin Drift

A spin-stabilized bullet develops a slow lateral drift in the direction of its spin. The empirical formula widely used for spin drift [Litz, 2011]:

$$\boxed{\Delta z_{\text{spin}} = 1.25 \, (S_g + 1.2) \cdot t^{1.83}} \tag{6.5}$$

where Δz_{spin} is the deflection in inches, S_g is the gyroscopic stability factor, and t is the time of flight in seconds.

6.2.1 Gyroscopic Stability Factor

The Miller stability formula [Miller, 2005]:

$$\boxed{S_g \approx \frac{30\,m}{T_w^2\,d^3\,l\,(1+l^2)} \cdot \frac{v_0}{2800} \cdot \frac{T_0}{T}} \tag{6.6}$$

where m is bullet mass in grains, T_w is twist rate in calibers per turn, d is caliber in inches, l is bullet length in calibers, $T_0 = 518.67$ R (59 °F).

For adequate stability, $S_g > 1.0$; values of 1.3–2.0 are typical for match bullets.

6.3 Coriolis and Eötvös Effects

6.3.1 Coriolis Acceleration

In an Earth-fixed reference frame:

$$\boldsymbol{a}_{\text{Cor}} = -2\,\boldsymbol{\omega}_E \times \boldsymbol{v} \tag{6.7}$$

where $\omega_E = 7.2921 \times 10^{-5}\ \frac{\text{rad}}{\text{s}}$.

6.3.2 Horizontal Deflection

$$\boxed{\Delta z_{\text{Cor}} \approx \omega_E \sin\phi \cdot R \cdot t} \tag{6.8}$$

Always to the right in the Northern Hemisphere, left in the Southern. At 45 N, 1000 yd, $t \approx 1.5$ s: $\Delta z \approx 2.8$ inches (≈ 0.27 MOA).

6.3.3 Vertical Deflection (Eötvös Effect)

$$\boxed{\Delta y_{\text{Eot}} \approx \omega_E \cos\phi \sin\psi \cdot R \cdot t} \tag{6.9}$$

Firing East ($\psi = 90°$) results in a positive vertical deflection (the bullet shoots higher due to the increased centrifugal force), while firing West ($\psi = 270°$) results in a negative deflection. At 45°N, 1000 yd, the effect is approximately ± 3 to 4 inches.

6.4 Aerodynamic Jump

For a spin-stabilized bullet with initial yaw α_0 [McCoy, 1999]:

$$\theta_{\text{jump}} = \frac{C_{L_\alpha}}{2\,k_t^2}\,\frac{\alpha_{\text{trim}}}{p_s - r_s} \tag{6.10}$$

In practice, aerodynamic jump is absorbed into zero-offset and has a random component that contributes to group size rather than a systematic bias.

6.5 Magnus Effect

$$F_{\text{Magnus}} = \frac{1}{2}\rho\,v^2\,A\,C_{N_{p\alpha}}\,\frac{p\,d}{2\,v}\,\alpha \tag{6.11}$$

For typical small yaw angles ($\alpha < 1$ deg), the Magnus contribution is sub-0.1 MOA at 1000 yd and is usually neglected.

Chapter 7

Complete 3-DOF Ballistic Solver

The complete 3-DOF ballistic solver is implemented in the companion file `CompetitionBallistics.jl` (see Appendix B). The solver includes: G1/G7 drag model interpolation from BRL tables, full RK4 integration of the 3-DOF equations, automatic zero-angle finding, Coriolis and Eötvös corrections, post-hoc spin drift, and wind deflection. The `ShotParameters` struct accepts all physical inputs (bullet mass, BC, muzzle velocity, atmospheric conditions, wind, latitude, twist rate, etc.) and the `solve_trajectory()` function returns a vector of `TrajectoryPoint` records containing time, position, velocity, Mach number, and kinetic energy at each integration step.

```
include("CompetitionBallistics.jl")
using .CompetitionBallistics.ExteriorBallistics

params = ShotParameters(
    mass_grains=140.0, caliber_in=0.264,
    bc=0.311, drag_model=:G7,
    muzzle_vel_fps=2700.0, zero_range_yd=100.0,
    wind_speed_mph=10.0, wind_angle_deg=90.0,
    target_range_yd=1000.0,
    twist_in=8.0, bullet_length_in=1.34,
)
trajectory_table(params, step_yd=100)
```

Listing 7.1: Example: running the solver

Chapter 8

Six-Degree-of-Freedom (6-DOF) Model

The 3-DOF point-mass model tracks only translational motion and uses empirical patches for spin drift, Magnus force, and aerodynamic jump. The 6-DOF model treats the bullet as a spinning rigid body with three translational and three rotational degrees of freedom, predicting yaw, precession, nutation, spin decay, and all gyroscopic phenomena from first principles. This chapter develops the full 6-DOF equations of motion and their Julia implementation.

8.1 State Vector and Reference Frames

8.1.1 Coordinate Systems

We require two frames:

- **Earth-fixed (inertial) frame** $\{O;\, \boldsymbol{e}_x, \boldsymbol{e}_y, \boldsymbol{e}_z\}$: x downrange, y up, z right. The 3-DOF frame from Chapter 5.
- **Body-fixed frame** $\{G;\, \boldsymbol{b}_1, \boldsymbol{b}_2, \boldsymbol{b}_3\}$: Origin at the center of mass G. $\boldsymbol{b}_1$ along the symmetry axis (nose-forward), $\boldsymbol{b}_2$ and $\boldsymbol{b}_3$ in the transverse plane.

8.1.2 Euler Angles and Orientation

The orientation of the body frame relative to the inertial frame is described by three Euler angles in the aerospace (yaw-pitch-roll) convention:

- ψ: yaw angle (rotation about $\boldsymbol{e}_y$)
- ϑ: pitch angle (rotation about intermediate axis)
- φ: roll (spin) angle (rotation about $\boldsymbol{b}_1$)

The rotation matrix from inertial to body frame is:

$$\boldsymbol{R} = \boldsymbol{R}_1(\varphi)\, \boldsymbol{R}_2(\vartheta)\, \boldsymbol{R}_3(\psi) \tag{8.1}$$

8.1.3 The 12-Component State Vector

The full state vector is:

$$\boldsymbol{Y} = \big(x,\ y,\ z,\ u,\ v,\ w,\ \varphi,\ \vartheta,\ \psi,\ p,\ q,\ r\big)^T \tag{8.2}$$

where (x, y, z) is position, (u, v, w) is velocity in the inertial frame, $(\varphi, \vartheta, \psi)$ are Euler angles, and (p, q, r) are angular velocity components in the body frame: p is the spin rate about $\boldsymbol{b}_1$, and q, r are pitch and yaw rates.

8.2 Translational Equations of Motion

Newton's second law in the inertial frame:

$$\boxed{m\,\frac{\mathrm{d}\boldsymbol{v}}{\mathrm{d}t} = \boldsymbol{F}_{\text{grav}} + \boldsymbol{F}_{\text{drag}} + \boldsymbol{F}_{\text{lift}} + \boldsymbol{F}_{\text{Magnus}} + \boldsymbol{F}_{\text{pitch damp}}} \tag{8.3}$$

8.2.1 Total Angle of Attack

The total angle of attack α_t is the angle between the velocity vector $\boldsymbol{v}$ and the body symmetry axis $\boldsymbol{b}_1$:

$$\alpha_t = \arccos\left(\frac{\boldsymbol{v}\cdot\boldsymbol{b}_1}{\|\boldsymbol{v}\|}\right) \tag{8.4}$$

For small angles, this decomposes into:

$$\alpha \approx \vartheta - \gamma \quad \text{(pitch-plane angle of attack)} \tag{8.5}$$
$$\beta \approx \psi_b - \psi_v \quad \text{(yaw-plane angle of attack)} \tag{8.6}$$

where γ is the flight path angle.

8.2.2 Aerodynamic Force Components

All forces are expressed in terms of dimensionless coefficients, reference area $A = \pi d^2/4$, and dynamic pressure $\bar{q} = \frac{1}{2}\rho v^2$:

Axial drag force (opposing velocity along the symmetry axis):

$$F_{\text{drag}} = -\bar{q}\,A\,C_{D_0}(Ma) - \bar{q}\,A\,C_{D_{\alpha^2}}(Ma)\,\alpha_t^2 \tag{8.7}$$

where C_{D_0} is the zero-yaw drag coefficient and $C_{D_{\alpha^2}}$ is the yaw-drag coefficient.

Normal (lift) force (perpendicular to the symmetry axis, in the yaw plane):

$$F_N = \bar{q}\,A\,C_{N_\alpha}(Ma)\,\alpha_t \tag{8.8}$$

where C_{N_α} is the normal force derivative (lift-curve slope).

Magnus force (perpendicular to both the spin axis and the velocity–axis plane):

$$F_{\text{Magnus}} = \bar{q}\,A\,C_{N_{p\alpha}}(Ma)\,\frac{p\,d}{2\,v}\,\alpha_t \tag{8.9}$$

8.3 Rotational Equations of Motion

The general rotational equation for a rigid body in compact tensor form is:

$$\boxed{\dot{\boldsymbol{\omega}} = \boldsymbol{I}^{-1}(\boldsymbol{M} - \boldsymbol{\omega}\times\boldsymbol{I}\,\boldsymbol{\omega})} \tag{8.10}$$

where $\boldsymbol{I}$ is the inertia tensor, $\boldsymbol{\omega} = (p, q, r)^T$ is the angular velocity in the body frame, and $\boldsymbol{M}$ is the total external moment. The cross-product term $\boldsymbol{\omega}\times\boldsymbol{I}\,\boldsymbol{\omega}$ represents the gyroscopic coupling.

For an axially symmetric projectile (body of revolution) with I_x (axial) and $I_y = I_z$ (transverse), the inertia tensor is diagonal and Eq. (8.10) expands to the scalar Euler equations:

$$I_x\,\dot{p} = M_x \tag{8.11}$$
$$I_y\,\dot{q} + (I_x - I_y)\,p\,r = M_q \tag{8.12}$$
$$I_y\,\dot{r} - (I_x - I_y)\,p\,q = M_r \tag{8.13}$$

8.3.1 Aerodynamic Moments

Overturning (pitching) moment — the moment that tends to increase the angle of attack:

$$M_{\text{pitch}} = \bar{q}\, A\, d\, C_{M_\alpha}(Ma)\, \alpha_t \tag{8.14}$$

where C_{M_α} is the pitching moment coefficient derivative. For statically stable configurations, $C_{M_\alpha} < 0$ (restoring moment). For bullets, $C_{M_\alpha} > 0$ (statically unstable; stability comes from spin).

Spin-damping moment — the torque that decelerates spin:

$$M_{\text{spin}} = \bar{q}\, A\, d^2\, C_{l_p}(Ma)\, \frac{p\, d}{2\, v} \tag{8.15}$$

where $C_{l_p} < 0$ is the spin-damping coefficient.

Pitch-damping moment — opposes pitch/yaw rate:

$$M_{\text{damp}} = \bar{q}\, A\, d^2\, \left(C_{M_q} + C_{M_{\dot{\alpha}}}\right)\, \frac{d}{2\, v}\, (q \text{ or } r) \tag{8.16}$$

Magnus moment:

$$M_{\text{Magnus}} = \bar{q}\, A\, d^2\, C_{M_{p\alpha}}(Ma)\, \frac{p\, d}{2\, v}\, \alpha_t \tag{8.17}$$

8.3.2 Summary of Moment Components

The total moments about each body axis:

$$M_x = \bar{q}\, A\, d^2\, C_{l_p}\, \frac{p\, d}{2v} \tag{8.18}$$

$$M_q = \bar{q}\, A\, d \left[C_{M_\alpha}\, \alpha - C_{M_{p\alpha}}\, \frac{pd}{2v}\, \beta + \left(C_{M_q} + C_{M_{\dot{\alpha}}}\right) \frac{qd}{2v}\right] \tag{8.19}$$

$$M_r = \bar{q}\, A\, d \left[C_{M_\alpha}\, \beta + C_{M_{p\alpha}}\, \frac{pd}{2v}\, \alpha + \left(C_{M_q} + C_{M_{\dot{\alpha}}}\right) \frac{rd}{2v}\right] \tag{8.20}$$

8.4 Kinematic Equations

The Euler angle rates relate to the body-frame angular velocities:

$$\dot{\varphi} = p + (q \sin\varphi + r \cos\varphi) \tan\vartheta \tag{8.21}$$

$$\dot{\vartheta} = q \cos\varphi - r \sin\varphi \tag{8.22}$$

$$\dot{\psi} = (q \sin\varphi + r \cos\varphi) \sec\vartheta \tag{8.23}$$

For small angles of attack ($\alpha_t < 10°$), typical of rifle bullets, these simplify considerably.

8.5 Quaternion Formulation (Singularity-Free)

The Euler-angle formulation has a singularity at $\vartheta = \pm 90°$ (gimbal lock). For robust numerical integration, the unit quaternion $\boldsymbol{q} = (q_0, q_1, q_2, q_3)^T$ is preferred:

$$\frac{\mathrm{d}}{\mathrm{d}t} \begin{pmatrix} q_0 \\ q_1 \\ q_2 \\ q_3 \end{pmatrix} = \frac{1}{2} \begin{pmatrix} 0 & -p & -q & -r \\ p & 0 & r & -q \\ q & -r & 0 & p \\ r & q & -p & 0 \end{pmatrix} \begin{pmatrix} q_0 \\ q_1 \\ q_2 \\ q_3 \end{pmatrix} \tag{8.24}$$

The rotation matrix from the quaternion:

$$\boldsymbol{R} = \begin{pmatrix} 1-2(q_2^2+q_3^2) & 2(q_1q_2-q_0q_3) & 2(q_1q_3+q_0q_2) \\ 2(q_1q_2+q_0q_3) & 1-2(q_1^2+q_3^2) & 2(q_2q_3-q_0q_1) \\ 2(q_1q_3-q_0q_2) & 2(q_2q_3+q_0q_1) & 1-2(q_1^2+q_2^2) \end{pmatrix} \tag{8.25}$$

After each RK4 step, renormalize: $\boldsymbol{q} \leftarrow \boldsymbol{q}/\|\boldsymbol{q}\|$.

8.6 Aerodynamic Coefficient Database

8.6.1 Typical Values for Match Bullets

The aerodynamic coefficients are functions of Mach number. Typical values for a 6.5 mm, 140 gr VLD match bullet at $Ma \approx 2.4$ (muzzle) [McCoy, 1999, Carlucci and Jacobson, 2007]:

Table 8.1: Typical aerodynamic coefficients for a 6.5 mm 140 gr VLD match bullet

Coefficient	Symbol	Typical Value	Description
Zero-yaw drag	C_{D_0}	0.15–0.30	From G7 table via BC
Yaw drag	$C_{D_{\alpha^2}}$	2.0–5.0	Drag increase with yaw
Lift-curve slope	C_{N_α}	2.0–3.5	Normal force per rad
Overturning moment	C_{M_α}	2.0–4.0	Destabilizing (positive)
Spin damping	C_{l_p}	-0.005 to -0.02	Retards spin
Pitch damping	$C_{M_q} + C_{M_{\dot\alpha}}$	-5 to -15	Damps yaw oscillation
Magnus force	$C_{N_{p\alpha}}$	-0.5 to $+0.5$	Cross-spin force
Magnus moment	$C_{M_{p\alpha}}$	-0.5 to $+0.5$	Cross-spin moment

[default: Values in the Julia implementation when not user-specified.]

8.6.2 Deriving C_{D_0} from the Ballistic Coefficient

The zero-yaw drag coefficient relates directly to the standard drag model and the ballistic coefficient:

$$C_{D_0}(Ma) = i \cdot C_D^{\text{std}}(Ma) = \frac{\text{SD}}{B_{\text{C}}} C_D^{\text{std}}(Ma) \tag{8.26}$$

This allows the 6-DOF model to use the same BC input as the 3-DOF model for the dominant drag term.

8.7 Moments of Inertia

For a rotationally symmetric bullet of mass m, length L, and diameter d:

$$I_x \approx \frac{1}{2} m r_g^2 \quad \text{(axial, about symmetry axis)} \tag{8.27}$$

$$I_y = I_z \approx m\left(\frac{L^2}{12} + \frac{r_g^2}{4}\right) \quad \text{(transverse)} \tag{8.28}$$

where $r_g = d/2$ is the radius of gyration. For a typical match bullet, $I_y/I_x \approx 5$–10.

8.8 Spin Rate and Initial Conditions

The initial spin rate from the barrel twist rate τ (inches/turn):

$$p_0 = \frac{2\pi\, v_0}{\tau} \tag{8.29}$$

For a 1:8 twist barrel at 2700 fps: $p_0 = 2\pi \times 2700/(8/12) = 2\pi \times 4050 \approx 25{,}447$ rad/s ($\approx 243{,}000$ RPM).

8.9 Stability Revisited from 6-DOF Theory

8.9.1 Gyroscopic Stability

From the linearized 6-DOF equations, the gyroscopic stability factor is rigorously:

$$S_g = \frac{I_x^2\, p^2}{2\,\rho\, A\, d\, I_y\, v^2\, C_{M_\alpha}} \tag{8.30}$$

This is the exact form from which the Miller approximation (Eq. 6.6) is derived.

8.9.2 Dynamic Stability

The dynamic stability factor from the 6-DOF linearization:

$$S_d = \frac{2\, C_{N_\alpha}}{C_{M_\alpha}} \cdot \frac{1}{S_g(S_g - 1)} \cdot \left(\frac{C_{N_\alpha} + \frac{2m}{\rho A d}\, k_t^2}{C_{M_q} + C_{M_{\dot\alpha}}} \right)^2 \tag{8.31}$$

Full stability requires $S_g > 1$ and $0 < S_d < 2$.

8.10 Comparison: 3-DOF vs. 6-DOF

Table 8.2: Comparison of 3-DOF and 6-DOF models

Feature	**3-DOF**	**6-DOF**
State variables	6 (position + velocity)	13 (+ quaternion + angular velocity)
Spin drift	Empirical (Litz formula)	Predicted from first principles
Yaw/precession	Not modeled	Fully resolved
Magnus force	Neglected or lumped	Computed from $C_{N_{p\alpha}}$
Transonic behavior	No yaw prediction	Predicts instability onset
Aerodynamic data	BC only	BC + 7 additional coefficients
Computation speed	$\sim$0.01 s	$\sim$0.1–0.5 s
Accuracy at 1000 yd	< 0.5 MOA (with corrections)	< 0.1 MOA

For most competition shooting, the 3-DOF model with empirical spin drift and Coriolis corrections is sufficient. The 6-DOF model is valuable for: bullet design evaluation, predicting transonic stability limits, understanding anomalous dispersion, and academic study.

8.11 Julia Implementation: 6-DOF Solver

The 6-DOF solver is implemented in the `SixDOF` module within `CompetitionBallistics.jl` (Appendix B). Key structures:

```
using .CompetitionBallistics.SixDOF

aero = AeroCoefficients6DOF(
    Cd0_func  = (Ma) -> cd_g7(Ma) * 1.02,  # from BC
    Cda2      = 3.5,        # yaw drag
    CNa       = 2.8,        # lift-curve slope
    CMa       = 3.2,        # overturning moment
    Clp       = -0.010,     # spin damping
    CMq_CMad  = -8.0,       # pitch damping sum
    CNpa      = 0.1,        # Magnus force
    CMpa      = -0.2,       # Magnus moment
)

params6 = ShotParameters6DOF(
    mass_grains=140.0, caliber_in=0.264,
    bullet_length_in=1.34,
    muzzle_vel_fps=2700.0, twist_in=8.0,
    initial_yaw_deg=0.5,  # typical muzzle yaw
    aero=aero,
)

traj = solve_6dof(params6)
```

Listing 8.1: 6-DOF solver usage example

Chapter 9

Angular Measurement and Sighting Systems

9.1 Minute of Angle (MOA)

$$1\ \text{MOA} = \frac{1}{60} \times \frac{\pi}{180} = 2.9089 \times 10^{-4}\,\text{rad} \tag{9.1}$$

The common approximation: 1 MOA ≈ 1.047 inches at 100 yd.

The angular correction in MOA for a vertical drop Δy at range R (assuming Δy and R are in the same units) is:

$$\boxed{\text{MOA} = \frac{\Delta y}{R} \cdot \frac{180 \times 60}{\pi} \approx \frac{\Delta y}{R} \cdot 3437.75} \tag{9.2}$$

9.2 Milliradian (Mil)

$$1\ \text{mil} = 0.001\,\text{rad} \approx 3.6 \text{ inches at } 100\,\text{yd} \tag{9.3}$$

Conversion: 1 mil = 3.438 MOA.

The angular correction in mils for a vertical drop Δy at range R (same units) is:

$$\boxed{\text{mil} = \frac{\Delta y}{R} \times 1000} \tag{9.4}$$

Chapter 10

Reloading Guide for Competition Shooters

Safety warning: Always cross-reference with current published load data. Start 10% below listed maximum charges and work up carefully.

10.1 Cartridge Selection for Competition

Table 10.1: Popular competition cartridges and their characteristics

Cartridge	Bullet (gr)	v_0 (fps)	BC (G7)	Barrel	Discipline
6mm BR	105–108	2850–2950	.225–.275	26–28	Benchrest, F-Class
6mm Creedmoor	105–115	2950–3100	.255–.290	26–28	PRS, NRL, F-Class
6mm Dasher	105–115	2950–3050	.225–.290	26–28	PRS, NRL
6.5 Creedmoor	130–147	2550–2800	.255–.340	24–26	PRS, NRL, F-Class
6.5×47 Lapua	130–147	2650–2850	.255–.340	26–28	Palma variant
.284 Win	180	2850–2950	.340–.365	28–30	F-Class Open
.308 Win	155–185	2550–2800	.220–.275	24–30	Palma, Tactical
.223 Rem	69–80	2700–3000	.145–.200	20–26	Service Rifle
.300 Win Mag	190–230	2800–3000	.310–.415	26–30	F-Class Open
.338 Lapua Mag	250–300	2700–2900	.370–.450	27–30	ELR

10.2 Propellant Selection

Table 10.2: Popular propellants for competition rifle cartridges

Propellant	Burn Rate	Temp Stable?	Typical Cartridges
Hodgdon Varget	Medium	Yes (Extreme)	.308, .223, 6.5 CM, 6BR
Hodgdon H4350	Med-slow	Yes (Extreme)	6.5 CM, 6 CM, .284, .260
Hodgdon H4895	Medium	Yes (Extreme)	6BR, .308, .223
Alliant RL-16	Med-slow	Yes (ETS)	6.5 CM, 6 CM, 6mm BR
Vihtavuori N140	Medium	Moderate	6mm BR, .308, .223
Vihtavuori N150	Med-slow	Moderate	6.5 CM, 6 CM, .260
Vihtavuori N555	Medium	Yes	6mm BR, 6 Dasher
Vihtavuori N565	Med-slow	Yes	6.5 CM, 6 CM, 6.5×47
IMR 4451	Med-slow	Yes (Enduron)	6.5 CM, 6 CM, .308

10.3 Representative Load Data

Disclaimer: Reference only. Always consult current manufacturer manuals. Start 10% below maximum.

Table 10.3: 6.5 Creedmoor representative loads (24-inch barrel)

Bullet	Propellant	Charge (gr)	COAL (in)	v_0 (fps)	Press.
140 Berger Hybrid	H4350	40.0–42.5	2.800	2650–2760	Near max
147 Hornady ELD-M	H4350	38.5–41.0	2.830	2550–2660	Near max
130 Berger Hybrid	H4350	41.0–43.5	2.810	2750–2880	Near max
140 Sierra MK	RL-16	39.0–41.5	2.800	2640–2750	Near max
147 Hornady ELD-M	N565	39.5–42.0	2.830	2570–2680	Near max

Table 10.4: .308 Winchester representative loads (24-inch barrel)

Bullet	Propellant	Charge (gr)	COAL (in)	v_0 (fps)	Press.
175 Sierra MK	Varget	42.0–44.5	2.800	2550–2680	Near max
155 Berger Hybrid	Varget	44.5–47.0	2.800	2750–2870	Near max
168 Sierra MK	Varget	43.0–45.5	2.800	2600–2720	Near max
175 Sierra MK	N150	43.0–45.0	2.800	2570–2670	Near max

Table 10.5: 6mm Creedmoor representative loads (26-inch barrel)

Bullet	Propellant	Charge (gr)	COAL (in)	v_0 (fps)	Press.
105 Berger Hybrid	H4350	39.5–42.0	2.800	3000–3100	Near max
108 Berger BT Tgt	H4350	39.0–41.5	2.800	2950–3070	Near max
115 Berger Hybrid	RL-16	38.0–40.5	2.810	2880–2990	Near max
105 Hornady ELD-M	N565	38.5–41.0	2.790	2980–3080	Near max
109 Berger LRHT	H4350	38.5–41.0	2.810	2950–3060	Near max

Table 10.6: 6mm BR Norma representative loads (26-inch barrel)

Bullet	Propellant	Charge (gr)	COAL (in)	v_0 (fps)	Press.
105 Berger Hybrid	Varget	29.0–30.5	2.350	2850–2950	Near max
105 Berger Hybrid	N140	29.5–31.0	2.350	2870–2960	Near max
108 Berger BT Tgt	Varget	28.5–30.0	2.350	2820–2920	Near max
108 Berger BT Tgt	N555	29.0–30.5	2.350	2850–2950	Near max
105 Lapua Scenar	H4895	28.5–30.0	2.340	2830–2930	Near max
107 Sierra MK	Varget	28.5–30.0	2.350	2830–2930	Near max

10.4 Complete Worked Example: 6mm BR at 1000 Yards

This section walks through a complete ballistic simulation for a 6mm BR Norma benchrest/F-Class load, from component data through atmospheric correction to a full trajectory table with all secondary effects. This serves as a template for any cartridge.

10.4.1 Step 1: Component Data

Our load:

- **Bullet:** Berger 105 gr Hybrid Target, 6mm (.243 cal)

- **BC (G7):** 0.275 [Litz, 2015]
- **Bullet length:** 1.10 in.
- **Propellant:** Vihtavuori N140, 30.2 gr
- **Muzzle velocity:** 2920 fps (from 26-inch barrel, verified by chronograph)
- **Barrel twist:** 1:7.5 right-hand
- **Brass:** Lapua 6mm BR, weight-sorted ±0.5 gr
- **Primer:** CCI BR-4 small rifle benchrest

10.4.2 Step 2: Stability Check

Using the Miller formula (Eq. 6.6):

$$d = 0.243 \text{ in.}, \quad l = 1.10/0.243 = 4.527 \text{ cal}, \quad T_w = 7.5/0.243 = 30.86 \text{ cal/turn}$$

$$\begin{aligned} S_g &= \frac{30 \times 105}{30.86^2 \times 0.243^3 \times 4.527 \times (1 + 4.527^2)} \times \frac{2920}{2800} \times \frac{518.67}{518.67} \\ &= \frac{3150}{30.86^2 \times 0.01435 \times 4.527 \times 21.49} \times 1.043 \\ &\approx 1.68 \end{aligned}$$

$S_g = 1.68 > 1.3$: well stabilized. The bullet will maintain gyroscopic stability down to approximately Mach 1.2 (about 1350 fps), which occurs near 1100 yards for this load.

10.4.3 Step 3: Atmospheric Conditions

Match day conditions (summer F-Class match in Ottawa, Canada):

$$T = 82\,^\circ\text{F} = 300.9 \text{ K}, \quad P = 29.75 \text{ in Hg} = 100\,750 \text{ Pa}$$
$$H = 55\%, \quad \text{Altitude} = 250 \text{ ft}$$

Air density from Eq. (2.11):

$$\begin{aligned} e_s &= 610.78 \times 10^{7.5 \times 27.7/(27.7+237.3)} = 3695 \text{ Pa} \\ e &= 0.55 \times 3695 = 2032 \text{ Pa} \\ \rho &= \frac{100\,750 - 0.3783 \times 2032}{287.058 \times 300.9} = \frac{99\,981}{86\,380} = 1.1575 \text{ kg/m}^3 \end{aligned}$$

Density ratio: $\rho/\rho_0 = 1.1575/1.2250 = 0.9449$. The air is 5.5% less dense than standard, so the bullet will retain velocity longer and shoot approximately 0.8 MOA flatter at 1000 yards compared to standard conditions.

Speed of sound: $a = 20.047\sqrt{300.9} = 347.7$ m/s.

Muzzle Mach number: $Ma_0 = 890.0/347.7 = 2.56$ (well into the supersonic regime).

10.4.4 Step 4: Solver Setup and Trajectory

The complete Julia solver call for this scenario:

```
params_6br = ShotParameters(
    # Bullet: Berger 105 Hybrid Target
    mass_grains     = 105.0,
    caliber_in      = 0.243,
    bc              = 0.275,        # G7
    drag_model      = :G7,
```

```
    # Launch
    muzzle_vel_fps  = 2920.0,
    sight_height_in = 1.5,
    zero_range_yd   = 100.0,

    # Atmosphere: Ottawa, summer match
    temp_F          = 82.0,
    pressure_inhg   = 29.75,
    humidity_pct    = 55.0,
    altitude_ft     = 250.0,

    # Wind: 8 mph from 2 o'clock (60 deg off nose)
    wind_speed_mph  = 8.0,
    wind_angle_deg  = 60.0,

    # Target
    target_range_yd = 1000.0,

    # Spin: 1:7.5 RH twist
    twist_in        = 7.5,
    twist_direction = 1,
    bullet_length_in = 1.10,

    # Location: Ottawa, ON
    latitude_deg    = 45.4,
    azimuth_deg     = 270.0,        # firing West
    enable_coriolis = true,
    enable_spin_drift = true,
)

trajectory_table(params_6br, step_yd=100)
```

Listing 10.1: 6mm BR complete trajectory example

The solver output for this configuration:

Table 10.7: Computed trajectory: 6mm BR, 105 gr Berger Hybrid, $v_0 = 2920$ fps, 82 °F, 29.75 in Hg, 55% RH. 8 mph wind at 60°. 100 yd zero. 1:7.5 RH twist, 45.4°N, firing West.

Range (yd)	Drop (in)	Elev (MOA)	Vel (fps)	Mach	Energy (ft-lb)	ToF (s)	Wind (in)	Spin (in)
100	0.0	0.0	2766	2.43	1784	0.106	0.3	0.0
200	−2.3	1.1	2617	2.30	1597	0.219	1.5	0.1
300	−9.0	2.9	2473	2.17	1427	0.339	3.6	0.2
400	−20.7	5.0	2334	2.05	1271	0.466	6.8	0.4
500	−38.2	7.3	2200	1.93	1129	0.602	11.1	0.7
600	−62.5	10.0	2070	1.82	1000	0.747	16.8	1.1
700	−94.8	12.9	1945	1.71	883	0.903	24.0	1.6
800	−136.5	16.3	1824	1.60	776	1.070	32.9	2.3
900	−189.5	20.1	1708	1.50	681	1.250	43.9	3.1
1000	−256.0	24.5	1596	1.40	594	1.445	57.0	4.1

10.4.5 Step 5: Analysis of Results

Velocity retention. The bullet arrives at 1000 yards at 1596 fps (Mach 1.40), still well above the transonic threshold (≈1340 fps). The 6mm BR with a high-BC 105 gr bullet retains adequate supersonic margin.

Total elevation. From the 100-yard zero, the shooter dials 24.5 MOA of elevation (approximately 7.1 mils). This is competitive with the 6.5 Creedmoor (28.5 MOA for 140 gr, Table 11.2) despite the lighter bullet, thanks to the higher muzzle velocity.

Wind deflection. The 8 mph wind at 60° produces a crosswind component $W_{\text{cross}} = 8 \sin 60° = 6.93$ mph and a headwind component $W_{\text{head}} = 8 \cos 60° = 4.0$ mph. The total wind deflection at 1000 yards is 57.0 inches (5.4 MOA). For a full-value 10 mph crosswind, this would scale to approximately 74 inches — about 4% more than the 6.5 Creedmoor (77.1 in.) but comparable, illustrating that the 6mm BR's higher velocity partly compensates for the lower BC.

Spin drift. The 1:7.5 RH twist produces 4.1 inches of rightward drift at 1000 yards (0.39 MOA). This is a systematic bias that should be dialed into the scope or included in the wind hold.

Coriolis and Eötvös. Firing West at 45.4°N latitude:

- Horizontal Coriolis: ≈ 2.7 inches right (0.26 MOA), same direction as spin drift.
- Eötvös (firing West): ≈ 3.4 inches *down* (the bullet loses the "boost" of the Earth's rotation), adding about 0.3 MOA to the required elevation.

Total horizontal correction: Wind 57.0 in. + spin drift 4.1 in. + Coriolis 2.7 in. = 63.8 inches total rightward deflection (6.1 MOA).

10.4.6 Step 6: Chronograph Validation

A 20-round chronograph string from this load:

2918, 2925, 2914, 2928, 2920, 2916, 2922, 2919, 2927, 2921,
2915, 2923, 2926, 2917, 2920, 2924, 2919, 2922, 2916, 2925

Statistics: $\bar{v} = 2920.9$ fps, ES = 14 fps, SD = 3.9 fps. The SD of 3.9 fps produces a vertical dispersion of:

$$\sigma_y(1000 \text{ yd}) \approx 0.23 \times 3.9 = 0.90 \text{ inches} \quad (0.09 \text{ MOA})$$

This is well below the F-Class X-ring diameter (2.5 inches) and represents a benchrest-grade load.

10.4.7 Step 7: DOPE Card Summary

Table 10.8: DOPE card: 6mm BR 105 Berger / N140 / 2920 fps. Ottawa, 82 °F, 29.75 inHg. Wind hold is per 1 mph full crosswind.

Range (yd)	Elevation (MOA)	Wind/1 mph (MOA)	Spin+Cor (MOA)
200	1.1	0.07	0.01
300	2.9	0.11	0.03
400	5.0	0.16	0.05
500	7.3	0.21	0.08
600	10.0	0.27	0.12
700	12.9	0.33	0.17
800	16.3	0.39	0.23
900	20.1	0.47	0.30
1000	24.5	0.54	0.39

This DOPE card gives the shooter all the information needed: dial the elevation, hold or dial the wind column multiplied by the estimated crosswind speed, and add the spin+Coriolis correction. The total process—from the mathematical models of Chapters 2–6 through the Julia solver of Chapter 7 to this practical output—represents the complete ballistic pipeline that this manual describes.

10.5 Interpreting Chronograph Data

$$\bar{v} = \frac{1}{N}\sum_{i=1}^{N} v_i, \qquad \text{ES} = v_{\max} - v_{\min}, \qquad \text{SD} = \sqrt{\frac{1}{N-1}\sum_{i=1}^{N}(v_i - \bar{v})^2} \tag{10.1}$$

Target values: ES $<$ 20 fps (excellent: $<$ 10), SD $<$ 8 fps (excellent: $<$ 4).

As a practical benchmark, the following table shows typical velocity consistency for factory versus hand-loaded ammunition:

Table 10.9: Typical velocity consistency: factory ammunition vs. optimized handloads

Ammunition type	ES (m/s)	ES (fps)
Standard factory match	9–10	30–33
Premium factory match	5–7	16–23
Optimized handloads	2–3	7–10
Benchrest-grade handloads	$<$2	$<$7

The gap between factory and hand-loaded ammunition is the primary motivation for reloading in competition shooting: reducing velocity spread by a factor of 3–5 translates directly into tighter vertical dispersion at long range (see below).

10.5.1 Velocity SD Impact on Vertical Dispersion

$$\sigma_y(R) \approx \left|\frac{\partial y}{\partial v_0}\right|_R \cdot \sigma_v \tag{10.2}$$

Chapter 11

Ballistic Reference Tables

11.1 Bullet Data for Common Competition Bullets

Table 11.1: Ballistic data for popular competition bullets [Litz, 2011, 2015]

Bullet	Wt (gr)	Cal	BC G1	BC G7	SD	Twist
Berger 105 Hyb 6mm	105	.243	0.536	0.275	0.254	1:7.5
Berger 140 Hyb 6.5	140	.264	0.607	0.311	0.287	1:8
Hornady 147 ELD-M	147	.264	0.697	0.351	0.301	1:7.5
Berger 180 Hyb 7mm	180	.284	0.683	0.350	0.319	1:8.5
Sierra 175 MK .308	175	.308	0.505	0.259	0.264	1:10
Berger 185 Jugg .308	185	.308	0.552	0.283	0.279	1:10
Hornady 178 ELD-M	178	.308	0.535	0.274	0.268	1:10
Berger 300 Hyb .338	300	.338	0.818	0.419	0.375	1:9.4

11.2 Sample Trajectory Table

Table 11.2: Trajectory: 6.5 CM, 140 gr Berger Hybrid, $BC_{G7} = 0.311$, $v_0 = 2700$ fps, 100 yd zero, sea level standard atmosphere

Range (yd)	Drop (in)	Come-Up (MOA)	Velocity (fps)	Energy (ft-lb)	ToF (s)	10 mph Wind (in)	Spin Drift (in)
100	0.0	0.0	2545	2015	0.115	0.5	0.0
200	−2.8	1.3	2396	1786	0.237	2.1	0.1
300	−10.7	3.4	2252	1578	0.365	5.0	0.3
400	−24.5	5.9	2113	1389	0.501	9.2	0.5
500	−45.0	8.6	1979	1219	0.646	15.1	0.9
600	−73.4	11.7	1851	1066	0.800	22.8	1.4
700	−111.0	15.1	1728	929	0.965	32.5	2.0
800	−159.5	19.0	1610	807	1.143	44.6	2.8
900	−221.1	23.5	1498	698	1.334	59.3	3.8
1000	−298.0	28.5	1393	604	1.541	77.1	5.1

Chapter 12

Special Topics

12.1 Transonic Stability

The dynamic stability factor S_d must be considered alongside S_g [McCoy, 1999]. For full stability: $S_g > 1.0$ and $0 < S_d < 2$.

As a bullet decelerates through the transonic zone ($0.9 \lesssim Ma \lesssim 1.2$), the centre of pressure shifts rapidly and the aerodynamic damping can change sign, potentially causing a well-stabilized supersonic bullet to become dynamically unstable. The practical consequence is increased dispersion—often dramatically so—once the bullet enters this regime. Long-range competitors should therefore know at what range their chosen load crosses into the transonic zone and treat that as the effective maximum range for precision fire.

Table 12.1: Approximate transonic transition ranges for common competition cartridges at sea-level standard conditions. The transonic zone is defined as $0.9 \leq Ma \leq 1.1$ ($\approx$ 310–380 $\frac{\text{m}}{\text{s}}$).

Cartridge	**Bullet (gr)**	v_0 **(m/s)**	**Enters transonic (m)**	**Subsonic (m)**
.223 Rem	77 SMK	838	≈600	≈750
.308 Win	155 Lapua Scenar	860	≈750	≈950
.308 Win	175 SMK	775	≈820	≈1075
6.5 Creedmoor	140 Berger Hybrid	823	≈950	≈1200
.300 Win Mag	185 Berger Jugg	943	≈1275	≈1600
.338 Lapua Mag	300 Berger Hybrid	838	≈1500	≈1900

Bullets with higher BC values and higher muzzle velocities remain supersonic longer, but the relationship is not linear: the steep drag rise in the transonic zone means that once a bullet begins to slow through $Ma \approx 1.1$, it decelerates rapidly. The solver in Chapter 7 captures this behavior through the fine resolution of the G7 drag table in the transonic region.

12.2 Inclined Fire (Rifleman's Rule)

$$R_{\text{effective}} = R_{\text{slant}} \cdot \cos\alpha \tag{12.1}$$

The perpendicular gravity component $g_\perp = g\cos\alpha$ causes the bullet to drop away from the line of sight. Since $\cos\alpha < 1$ for any nonzero inclination (up or down), the drop is always less than flat fire.

12.3 Barrel Harmonics and Optimal Charge Weight

Barrel vibrations cause the muzzle to describe an elliptical pattern at the moment of bullet exit. The OCW method seeks charge weights where the muzzle vertical angle is at an

extremum, creating a flat spot that compensates for velocity variation.

Chapter 13

Error Budget and Sensitivity Analysis

13.1 Sensitivity Coefficients

For any trajectory output Y at range R:

$$S_i = \frac{\partial Y}{\partial p_i} \approx \frac{Y(p_i + \Delta p_i) - Y(p_i - \Delta p_i)}{2\,\Delta p_i} \tag{13.1}$$

Table 13.1: Error budget: 6.5 Creedmoor, 140 gr, $\mathrm{BC_{G7}} = 0.311$, 2700 fps at 1000 yd

Parameter	**Uncertainty**	**Vertical (in)**	**Horizontal (in)**
Muzzle velocity	±10 fps	2.5	—
BC	±3%	3.2	1.8 (wind)
Wind speed (10 mph cross)	±2 mph	—	15.4
Wind direction	±10°	—	6.8
Temperature	±10 °F	0.8	—
Range estimation	±5 yd	1.5	—
Spin drift (uncompensated)	—	—	5.1
Coriolis (45°N, uncomp.)	—	<1.0	2.8

Key insight: Wind reading dominates the error budget at long range. Wind-related errors are 3–5 times larger than all other sources combined.

Chapter 14

Ballistic Implications for Reloading

This chapter bridges the mathematical models of the preceding chapters with the practical decisions a competition handloader must make at the reloading bench.

14.1 The Reloader's Equation: What You Control

From the 3-DOF equation of motion (Eq. 5.21), the trajectory depends on three groups of quantities:

1. **Bullet parameters** (m, d, B_C, L): fixed once the bullet is selected.
2. **Launch parameters** (v_0, σ_v, α_0): directly controlled by propellant charge, seating depth, neck tension, primer choice, and case preparation.
3. **Environmental parameters** (ρ, T, P, H, wind): not controllable, but the reloader can minimize their *impact* through component choices that reduce trajectory sensitivity.

14.2 Muzzle Velocity: The Central Reloading Output

14.2.1 Charge Weight and Velocity

The relationship between propellant charge weight C and muzzle velocity v_0 is approximately linear over the useful loading range:

$$v_0 \approx v_{\text{base}} + k_C\,(C - C_{\text{base}}) \tag{14.1}$$

where k_C is the velocity gain per grain, typically 15–40 fps/gr. For 6.5 Creedmoor with H4350, $k_C \approx 25$ fps/gr [Litz, 2011].

14.2.2 Velocity Consistency and Vertical Dispersion

From Eq. (10.2), the vertical group size at range R due to velocity variation:

$$\sigma_y(R) = \left|\frac{\partial y}{\partial v_0}\right|_R \cdot \sigma_v \tag{14.2}$$

Table 14.1: Velocity sensitivity: vertical shift per 1 fps change, 6.5 CM 140 gr

Range (yd)	$\lvert\partial y/\partial v_0\rvert$ **(in/fps)**	**Vertical for SD=10 fps (in)**
300	0.02	0.2
600	0.08	0.8
800	0.15	1.5
1000	0.25	2.5
1200	0.40	4.0
1500	0.72	7.2

14.2.3 Achieving Low SD: Quantitative Checklist

Assuming independent error sources, the combined SD is:

$$\sigma_{v,\text{total}} = \sqrt{\sigma^2_{\text{charge}} + \sigma^2_{\text{brass}} + \sigma^2_{\text{primer}} + \sigma^2_{\text{seat}} + \sigma^2_{\text{neck}} + \sigma^2_{\text{lot}}} \tag{14.3}$$

Table 14.2: Estimated velocity SD contributions by reloading variable

Variable	**Typical σ (fps)**	**Careful prep (fps)**
Charge weight (±0.1 gr thrown)	6–12	2–4 (weighed ±0.02 gr)
Brass volume variation (unsorted)	4–8	1–2 (sorted)
Primer seating depth variation	2–5	1–2 (uniformed pockets)
Seating depth variation	2–4	<1 (consistent BTO)
Neck tension variation	2–6	1–2 (turned, annealed)
Propellant lot variation	0–3	0 (single lot)
RSS total (typical)	**9–17**	
RSS total (prepared)		**3–5**

14.3 BC Sensitivity and Bullet Selection

A 10% higher BC reduces wind deflection by approximately 8–12%. **Choosing the highest-BC bullet your twist rate can stabilize is the single most impactful choice for reducing wind sensitivity**, which is the dominant error source (Table 13.1).

14.4 Temperature Effects: Propellant and Atmosphere

14.4.1 Combined Temperature Effect

$$\boxed{\Delta y_{\text{total}}(R, \Delta T) = \underbrace{\frac{\partial y}{\partial v_0}\,\sigma_T\,\Delta T}_{\text{velocity effect}} + \underbrace{\frac{\partial y}{\partial \rho}\,\frac{\partial \rho}{\partial T}\,\Delta T}_{\text{density effect}}} \tag{14.4}$$

For temperature-sensitive propellants, the two effects are *additive*. Using a temperature-stable propellant is ballistically equivalent to reducing the effective sensitivity by 60–80%.

Table 14.3: Temperature sensitivity by propellant class

Propellant Class	**σ_T (fps/°F)**	**Δv_0 for ±40 °F**
Standard (IMR 4064, etc.)	1.5–2.0	±60–80 fps
Temperature-stable (Varget, H4350)	0.3–0.8	±12–32 fps
Highly stable (RL-16, N565)	0.2–0.5	±8–20 fps

14.5 Seating Depth and Internal Ballistic Coupling

Seating depth affects freebore volume (pressure curve), engraving resistance (pressure peak timing), and initial alignment (reducing α_0). The empirical relationship:

$$\frac{\partial v_0}{\partial(\text{jump})} \approx -3 \text{ to } -8 \text{ fps per } 0.001 \text{ in. increase} \tag{14.5}$$

The group size model:

$$G(j) = \sqrt{G_{\text{base}}^2 + G_\alpha^2(j) + G_v^2(j)} \tag{14.6}$$

Typical sweet spots: jam/light contact (0.000–0.005 in.), moderate jump (0.015–0.030 in.), and extended jump (0.060–0.100 in.) [Litz, 2011].

14.6 Pressure Estimation and Safety Margins

Table 14.4: SAAMI maximum average pressure for competition cartridges

Cartridge	**MAP (psi)**	**MAP (MPa)**
.223 Remington	55,000	379
6.5 Creedmoor	62,000	427
.308 Winchester	62,000	427
.300 Winchester Magnum	64,000	441
.338 Lapua Magnum	60,916	420

From the Le Duc model peak pressure (Eq. 3.11):

$$P_{\text{peak}} \approx 1.6 \times P_{\text{avg}} = 1.6 \times \frac{m_e\, v_0^2}{2\, A_{\text{bore}}\, L_{\text{travel}}} \tag{14.7}$$

14.7 Barrel Life

Table 14.5: Approximate barrel life for competition cartridges

Cartridge	**Barrel Life (rounds)**
6mm BR / 6 Dasher	2500–3500
6.5 Creedmoor	2500–3000
.308 Winchester	5000–8000
.284 Winchester	1500–2500
.300 Winchester Magnum	1200–2000

The ballistic signature of barrel wear:

$$v_0(N) \approx v_{0,\text{new}} - k_{\text{wear}} \cdot N^{0.7} \tag{14.8}$$

$$\sigma_v(N) \approx \sigma_{v,\text{new}} + k_\sigma \cdot N^{0.5} \tag{14.9}$$

14.8 Load Development Workflow

Based on the mathematical models above:

Step 1: Bullet selection. Maximize B_{C}. Verify $S_g > 1.4$ using Eq. (6.6).

Step 2: Propellant selection. Temperature-stable. Calculate Δv_0 over competition temperature range using Eq. (3.13).

Step 3: Brass preparation. Sort by weight/capacity. Uniform necks and primer pockets.

Step 4: Charge weight exploration. Satterlee ladder or OCW test. Identify velocity nodes.

Step 5: Seating depth optimization. Test at 0.010 in. increments from lands.

Step 6: Validation. 20+ rounds over chronograph. SD < 8 fps (target < 5). Run the solver (Chapter 7) to verify vertical dispersion at max range.

Step 7: Temperature verification. Compute come-up shift using Eq. (14.4).

Appendix A

Detailed Mathematical Derivations

A.1 Derivation of the Point-Mass Equations of Motion

Starting from Newton's second law, neglecting lift (valid for small yaw):

$$m\,\ddot{\boldsymbol{r}} = -m\,g\,\hat{\boldsymbol{e}}_y - \frac{1}{2}\,\rho\,C_{\mathrm{D}}\,A\,\|\boldsymbol{v}_{\mathrm{rel}}\|\,\boldsymbol{v}_{\mathrm{rel}} \tag{A.1}$$

Expressing in component form with $\boldsymbol{v}_{\mathrm{rel}} = \boldsymbol{v} - \boldsymbol{v}_w$ and dividing by m, introducing $C_{\mathrm{D}}\,A/(2m) = \pi\,C_{\mathrm{D}}^{\mathrm{std}}/(8\,B_{\mathrm{C}})$, recovers Eqs. (5.22)–(5.24).

A.2 Derivation of the Coriolis Terms

In a rotating reference frame:

$$m\,\boldsymbol{a}_{\mathrm{rot}} = \boldsymbol{F} - 2m\,(\boldsymbol{\omega} \times \boldsymbol{v}_{\mathrm{rot}}) - m\,\boldsymbol{\omega} \times (\boldsymbol{\omega} \times \boldsymbol{r}) \tag{A.2}$$

The centrifugal term is absorbed into local g. In local coordinates at latitude ϕ:

$$\boldsymbol{\omega} = \omega_E\,(0, \cos\phi, \sin\phi)^T \tag{A.3}$$

Computing the cross product, the dominant terms for $v_x \gg v_y, v_z$ (where x is downrange, y is vertical, and z is cross-range):

$$a_z^{\mathrm{Cor}} \approx 2\omega_E\,v_x \sin\phi \tag{A.4}$$

$$a_y^{\mathrm{Cor}} \approx 2\omega_E\,v_x \cos\phi \sin\psi \tag{A.5}$$

where ψ is the firing azimuth. Integrating these twice with respect to time yields the deflection approximations used in Chapter 6.

A.3 Derivation of Spin Drift via Yaw of Repose

The equilibrium yaw angle from gyroscopic precession:

$$\alpha_{\mathrm{repose}} = \frac{g}{v^2} \cdot \frac{I_x\,\omega_s}{C_{M_\alpha}\,\frac{1}{2}\rho\,v^2\,A\,d} \tag{A.6}$$

This produces $F_{\mathrm{side}} = C_{L_\alpha}\,\frac{1}{2}\rho\,v^2\,A\,\alpha_{\mathrm{repose}}$, causing the spin drift deflection.

Appendix B

Companion Julia Package

The complete Julia implementation of all mathematical models in this manual is provided as a standalone file: `CompetitionBallistics.jl`. This file contains six sub-modules:

1. `BallisticUtils` — Unit conversions, sectional density, form factor, Miller stability, Greenhill twist.
2. `Atmosphere` — ICAO standard atmosphere, humidity correction, density altitude.
3. `InteriorBallistics` — Le Duc model, burn fraction, barrel length correction, temperature sensitivity, closed-bomb pressure.
4. `DragModels` — G1 and G7 BRL tabular data with both linear and cubic spline interpolation.
5. `ExteriorBallistics` — Full 3-DOF RK4 solver with wind, Coriolis, spin drift, zero-finding, and trajectory table output.
6. `ReloadingAnalysis` — Chronograph statistics, velocity-induced vertical dispersion, ladder test analysis, seating depth sensitivity, temperature shift tables, BC estimation from two chronographs, load quality scoring.

```
include("CompetitionBallistics.jl")
using .CompetitionBallistics
using .CompetitionBallistics.ExteriorBallistics
using .CompetitionBallistics.ReloadingAnalysis

params = ShotParameters(
    mass_grains=140.0, caliber_in=0.264,
    bc=0.311, drag_model=:G7,
    muzzle_vel_fps=2700.0, zero_range_yd=100.0,
    wind_speed_mph=10.0, wind_angle_deg=90.0,
    target_range_yd=1000.0,
    twist_in=8.0, bullet_length_in=1.34,
)
trajectory_table(params, step_yd=100)

# Chronograph analysis
v = [2695, 2702, 2688, 2710, 2699, 2693, 2701, 2707]
stats = chronograph_stats(v)
vert = velocity_vertical_dispersion(params, stats.sd,
                                    range_yd=1000.0)
```

Listing B.1: Quick-start usage of CompetitionBallistics.jl

The file requires only the Julia standard library (`Statistics`, `Printf`).

Appendix C

Greenhill's Formula and Twist Rate Selection

$$\boxed{T = \frac{C\,d^2}{l}\sqrt{\frac{\rho_b}{\rho_a}}} \tag{C.1}$$

For lead-core jacketed bullets, the simplified form: $T \approx 150\,d^2/l$.

Use $C = 150$ for $v < 2800$ fps, $C = 180$ for $v > 2800$ fps [Greenhill, 1879].

Stability guidance: $S_g < 1.0$ (unstable), 1.0–1.3 (marginal), 1.3–2.0 (optimal), > 2.0 (over-stabilized).

Bibliography

Bashforth, F. (1870). *A Mathematical Treatise on the Motion of Projectiles*. Asher & Co., London.

Braun, W.F. (1958). The free flight aerodynamics range. *Ballistic Research Laboratories Report No. 1048*. Aberdeen Proving Ground, MD.

Carlucci, D.E. and Jacobson, S.S. (2007). *Ballistics: Theory and Design of Guns and Ammunition*. CRC Press.

Greenhill, A.G. (1879). On the rotation required for the stability of an elongated projectile. *Minutes of the Proceedings of the Royal Artillery Institution*, 10:577–593.

International Civil Aviation Organization (1993). *Manual of the ICAO Standard Atmosphere*. ICAO Doc 7488/3, 3rd edition.

Ingalls, J.M. (1893). *Exterior Ballistics in the Plane of Fire*. D. Van Nostrand Company.

Litz, B. (2011). *Applied Ballistics for Long Range Shooting*. Applied Ballistics, LLC, 2nd edition.

Litz, B. (2015). *Ballistic Performance of Rifle Bullets*. Applied Ballistics, LLC, 3rd edition.

McCoy, R.L. (1999). *Modern Exterior Ballistics*. Schiffer Publishing, 2nd edition.

Miller, D. (2005). The new twist rule. *Precision Shooting*, March 2005.

Press, W.H. et al. (2007). *Numerical Recipes*. Cambridge University Press, 3rd edition.

Siacci, F. (1888). *Balistica*. Arnaldo Forni Editore, Bologna.

Glossary

BC	Ballistic Coefficient — ratio of sectional density to form factor.
BRL	Ballistic Research Laboratory (US Army, Aberdeen Proving Ground).
COAL	Cartridge Overall Length.
BTO	Base To Ogive length.
DA	Density Altitude.
ELR	Extreme Long Range ($>$ 1500 yd).
ES	Extreme Spread (max velocity $-$ min velocity).
MOA	Minute of Angle ($\approx$ 1.047 in. at 100 yd).
Mil	Milliradian ($\approx$ 3.6 in. at 100 yd).
OCW	Optimal Charge Weight.
PRS	Precision Rifle Series.
NRL	National Rifle League.
SD	Sectional Density or Standard Deviation (context-dependent).
VLD	Very Low Drag (bullet design).
S_g	Gyroscopic Stability Factor.
G1/G7	Standard drag model designations.